PLASMA ASTROPHYSICS

Direct measurements of two-way wave-particle energy transfer in a collisionless space plasma

N. Kitamura[1,2]*, M. Kitahara[3], M. Shoji[4], Y. Miyoshi[4], H. Hasegawa[1], S. Nakamura[5], Y. Katoh[3], Y. Saito[1], S. Yokota[6], D. J. Gershman[7], A. F. Vinas[7,8], B. L. Giles[7], T. E. Moore[7], W. R. Paterson[7], C. J. Pollock[9], C. T. Russell[10], R. J. Strangeway[10], S. A. Fuselier[11,12], J. L. Burch[11]

Particle acceleration by plasma waves and spontaneous wave generation are fundamental energy and momentum exchange processes in collisionless plasmas. Such wave-particle interactions occur ubiquitously in space. We present ultrafast measurements in Earth's magnetosphere by the Magnetospheric Multiscale spacecraft that enabled quantitative evaluation of energy transfer in interactions associated with electromagnetic ion cyclotron waves. The observed ion distributions are not symmetric around the magnetic field direction but are in phase with the plasma wave fields. The wave-ion phase relations demonstrate that a cyclotron resonance transferred energy from hot protons to waves, which in turn nonresonantly accelerated cold He^+ to energies up to ~2 kilo–electron volts. These observations provide direct quantitative evidence for collisionless energy transfer in plasmas between distinct particle populations via wave-particle interactions.

Wave-particle interactions are thought to play a crucial role in energy transfer in collisionless space plasmas in which the motion of charged particles is controlled by electromagnetic fields. In Earth's magnetosphere, electrons with energies on the order of a few to several tens of kilo–electron volts spontaneously generate electromagnetic electron cyclotron waves, called chorus emissions. Cyclotron resonant interaction with such waves and the resulting acceleration of electrons with energies on the order of several hundred kilo–electron volts are a leading candidate for the generation of relativistic electrons (on the order of mega–electron volts), which constitute the Van Allen radiation belt (*1*–*3*). Electromagnetic waves near the ion cyclotron frequency can accelerate ions through cyclotron resonance in the polar region (*4*), leading to the loss of O^+ from Earth's atmosphere. Electromagnetic ion cyclotron (EMIC) waves, generated spontaneously by hot ions in the equatorial magnetosphere, can cause loss of energetic ions via cyclotron resonant scattering, contributing to decay of geomagnetic storms (*5*). These waves can also induce quick loss of "satellite-killer" mega–electron volt electrons in the radiation belts during geomagnetic storms, limiting the threat that they pose to satellites (*6*, *7*). A quantitative understanding of wave-particle interactions and energy transfer between particle populations would therefore inform various space plasma phenomena such as the radiation belt, geomagnetic storms, auroral particle precipitation, and atmospheric loss from planets.

The coexistence of waves and accelerated particles (or particle populations that have free energy for wave growth) has been studied for decades in the magnetosphere (*8*–*10*). However, such coexistence does not necessarily indicate that energy is transferred between them at the observation site and time. In most situations, moving particles interact gradually with propagating waves in a spatially extended region, and it is not realistic to track a certain particle or wave packet with spacecraft. Thus, detecting local energy transfer between the fields and particles is necessary to quantitatively evaluate the magnitude of any interaction. Flux modulation of auroral precipitating electrons that may be related to cyclotron interactions with electrostatic waves was detected in the ionosphere (*11*). For direct quantitative measurements of the energy exchange between particle and electromagnetic waves via cyclotron interactions, the Wave-Particle Interaction Analyzer method that uses observed waveform and nonuniformity of particles around the magnetic field lines was proposed (*12*, *13*). Using this method, the detection of energy transfer from ions to waves via nonlinear cyclotron interactions has been achieved recently with in situ measurements with a temporal resolution of ~40 wave periods (*14*). However, the limited field of view and temporal resolution of their ion detectors did not allow observation of details of the interaction during the course of wave evolution (growth or decay), as characterized by temporal variations of the wave amplitude. We present direct evidence of energy transfer between two distinct particle populations through two concurrent cyclotron interactions based on quantitative measurements of the interactions, with a temporal resolution as high as one wave period.

The four Magnetospheric Multiscale (MMS) spacecraft (*15*) observed EMIC waves around 12:20 universal time (UT) on 1 September 2015 in the dusk-side magnetosphere (Fig. 1A and fig. S1). Because the spacecraft separation was smaller than both the wavelength estimated from the dispersion relation (fig. S2) and the cyclotron radius of hot H^+ (*16*), we use data averaged over all four spacecraft unless otherwise noted. We used the background magnetic field ($\mathbf{B}_0$) (<0.05 Hz) to define the magnetic field–aligned coordinates. The wave component of the magnetic field in the frequency range from 0.05 to 0.15 Hz, which is around the peak of the wave power (fig. S3), was derived as the wave magnetic field ($\mathbf{B}_{wave}$) (Fig. 2A). The perpendicular component of the wave electric field ($\mathbf{E}_{wave}$) in the same frequency range (Fig. 2B) was derived from cold ion motion (*16*). The field-aligned component of the Poynting flux [$\mathbf{S} = (\mathbf{E}_{wave} \times \mathbf{B}_{wave})/\mu_0$, where μ_0 is the vacuum permeability] was negative for most of the time interval, so the wave was propagating antiparallel to $\mathbf{B}_0$ (Figs. 1B and 2C).

The energy transfer rate via cyclotron-type interactions between cyclotron waves and ions was calculated as the dot product of $\mathbf{E}_{wave}$ and the ion current ($\mathbf{j}_i$) perpendicular to $\mathbf{B}_0$. In the case of resonant interactions between ions and waves, the current is called the resonant current (*17*). Over several energy and pitch-angle ranges, $\mathbf{j}_i$ was calculated by using burst data from the Fast Plasma Investigation Dual Ion Spectrometer (FPI-DIS) on MMS (*18*) with a time resolution of 150 ms, which is ~1/100 of the wave period (*16*). In a magnetized plasma, we expect the particles to be uniformly distributed around the magnetic field lines and call this uniformity "gyrotropy." The measured nonuniformity, or agyrotropy of ions, corresponding to $\mathbf{j}_i \neq 0$ causes an imbalance between the ions accelerated and decelerated by $\mathbf{E}_{wave}$, if $\mathbf{j}_i \cdot \mathbf{E}_{wave} \neq 0$. Thus, the agyrotropy and $\mathbf{j}_i \cdot \mathbf{E}_{wave}$ determine the net energy transfer for each part of the energy and pitch-angle ranges. Although this concept is the same as the Wave-Particle Interaction Analyzer method developed and used in previous works (*12*–*14*), the full-sky field of view of FPI-DIS enabled fast measurements of instantaneous $\mathbf{j}_i$ and thus of energy transfer rate ($\mathbf{j}_i \cdot \mathbf{E}_{wave}$).

First-order cyclotron resonance occurs when the resonance condition $V_{R\_i} = (\omega - \Omega_i)/k_{para}$ is satisfied, where V_{R_i} is the resonance velocity for ions, ω is the angular frequency of the left-hand polarized cyclotron wave, Ω_i is the ion

[1]Institute of Space and Astronautical Science, Japan Aerospace Exploration Agency, Sagamihara, Japan. [2]Department of Earth and Planetary Science, Graduate School of Science, the University of Tokyo, Tokyo, Japan. [3]Department of Geophysics, Graduate School of Science, Tohoku University, Sendai, Japan. [4]Institute for Space-Earth Environmental Research (ISEE), Nagoya University, Nagoya, Japan. [5]Research Institute for Sustainable Humanosphere (RISH), Kyoto University, Uji, Japan. [6]Department of Earth and Space Science, Graduate School of Science, Osaka University, Toyonaka, Japan. [7]NASA Goddard Space Flight Center, Greenbelt, MD, USA. [8]Department of Physics, American University, Washington, DC, USA. [9]Denali Scientific, Fairbanks, AK, USA. [10]Institute of Geophysics and Planetary Physics, University of California, Los Angeles, CA, USA. [11]Southwest Research Institute, San Antonio, TX, USA. [12]University of Texas at San Antonio, San Antonio, TX, USA.
***Corresponding author. Email: kitamura@eps.s.u-tokyo.ac.jp**

cyclotron frequency, and k_{para} is the wave number parallel to $\mathbf{B}_0$. The subscripts i indicate H^+ or He^+ ions. This condition is met when the angular frequency of $\mathbf{E}_{wave}$ and $\mathbf{B}_{wave}$ seen by ions with a parallel velocity V_{R_i} becomes equal to Ω_i because of the Doppler shift. In the MMS observation considered here, because the wave was propagating antiparallel to $\mathbf{B}_0$ and $\omega < \Omega_{He+}$, the resonance condition can be satisfied for H^+ or He^+ with pitch angles smaller than 90°.

Around 12:18:30 UT, 15-s averages of $\mathbf{j}_i \cdot \mathbf{E}_{wave}$ reached –0.3 pW m^{-3} for ions with energies 14 to 30 keV and pitch angles 33.25° to 78.75° (Fig. 2D), where the resonance condition for H^+ was satisfied. We confirmed that H^+ is the dominant ion species in this energy range (fig. S3) (*16*). For ions with pitch angles 101.25° to 146.75°, which did not satisfy the resonance condition, the averaged $\mathbf{j}_i \cdot \mathbf{E}_{wave}$ stayed much closer to zero (Fig. 2D), even though the pitch-angle distributions of the ions were almost symmetric about 90° (Fig. 2E). These results demonstrate that the energy of H^+ was being transferred to the cyclotron wave by the cyclotron resonance. These features were consistently observed by each of the four spacecraft, attesting to the robustness of the results (fig. S4).

A gyro phase versus time plot of differential energy fluxes is shown in Fig. 2F for ions with energies 14 to 30 keV and pitch angles 33.25° to 78.75°. To emphasize the agyrotropy, we normalized the values using the gyro-averaged values at each time (Fig. 2G). Two types of agyrotropy were seen. The first is stable in gyro angle (~12:17:20 to 12:18:10 and ~12:21:00 to 12:22:10 UT) and is related to the spatial gradient of ion fluxes, and the second is rotating (~12:18:10 to 12:19:15 UT). In the former case, $\mathbf{j}_i \cdot \mathbf{E}_{wave}$ cancels out over one complete wave period, and so the agyrotropy does not contribute to the net energy transfer. The latter case was investigated in more detail, by sorting the data using the relative phase angle (ζ), which is the gyro phase relative to the rotating $\mathbf{B}_{wave}$ (fig. S5). The resulting ζ versus time plot is shown in Fig. 2H. Relatively low ion fluxes were detected near the direction parallel to, and relatively high ion fluxes were detected near the direction antiparallel to, $\mathbf{E}_{wave}$, which remained at ζ ~ 90° around 12:18:10 to 12:18:45 UT. This agyrotropy rotating with $\mathbf{B}_{wave}$ and $\mathbf{E}_{wave}$ leads to the negative $\mathbf{j}_i \cdot \mathbf{E}_{wave}$ (Fig. 2D). Above 14 keV, a significant dip (~20 to 50% decrease from peak flux) at ζ ~ 90° can be seen in multiple pitch-angle bins, each consisting of individual measurements, in the ζ distribution of the differential energy fluxes (Fig. 3, A to D). As a quantitative measure of energy transfer, we computed gyro phase-averaged energy gain per H^+ ion perpendicular to $\mathbf{B}_0$ for each bin by dividing $\mathbf{j}_i \cdot \mathbf{E}_{wave}$ by the partial number density (Fig. 3E). Energy loss rates (negative energy gain) of up to ~80 eV s^{-1} per H^+ ion were identified around the H^+ resonance velocity $V_{R_{H^+}}$ = ~870 to 1720 km s^{-1}, which was derived by using the dispersion relation (*16*). This energy loss is due to the agyrotropic distribution shown in Fig. 3, A to D. Because $|\mathbf{B}_{wave}|$ reached ~10% of $|\mathbf{B}_0|$ in this event, the observed wide extent of the interactions around $V_{R_{H^+}}$ is consistent (*16*) with the nonlinear trapping of H^+ by the large-amplitude cyclotron wave (*17*).

Shortly after the beginning of the wave (~12:18:24 UT), He^+ with a peak at ~1.5 keV was detected in ion composition data (Fig. 4, A and B). This coincides with an ion population observed with FPI-DIS in the corresponding energy range that is concentrated in pitch angle between 90° and 112.5° (Fig. 4, C and D). These ions were concentrated in less than four 11.25° gyro phase bins and were rotating with the wave—they were phase-bunched (Fig. 4, D and E). The maximum energy of He^+ (~3 keV) is nearly equal to those in the most energetic He^+ energization event (~2 keV) that have been reported in the magnetosphere (*19*) and ~10 times

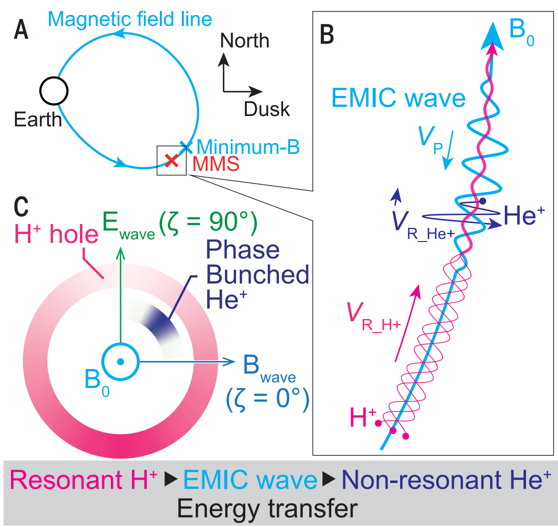

Fig. 1. Schematic diagrams summarizing EMIC wave propagation (direction of the phase velocity V_P), ion motion along the field line, and relative phase ζ distributions of He^+ and resonant H^+. (**A**) Positions of the MMS spacecraft and the point of lowest magnetic field (minimum-B). (**B** and **C**) Schematic of (B) the observed interactions and (C) ζ distributions of the phase-bunched He^+ with a small parallel velocity opposite to the He^+ resonance velocity $V_{R_{He^+}}$ and resonant H^+ with a parallel velocity equal to the H^+ resonance velocity $V_{R_{H^+}}$. Directions of the wave magnetic field $\mathbf{B}_{wave}$ and wave electric field $\mathbf{E}_{wave}$ relative to the background magnetic field $\mathbf{B}_0$, which is directed out of the page, are also shown in (C).

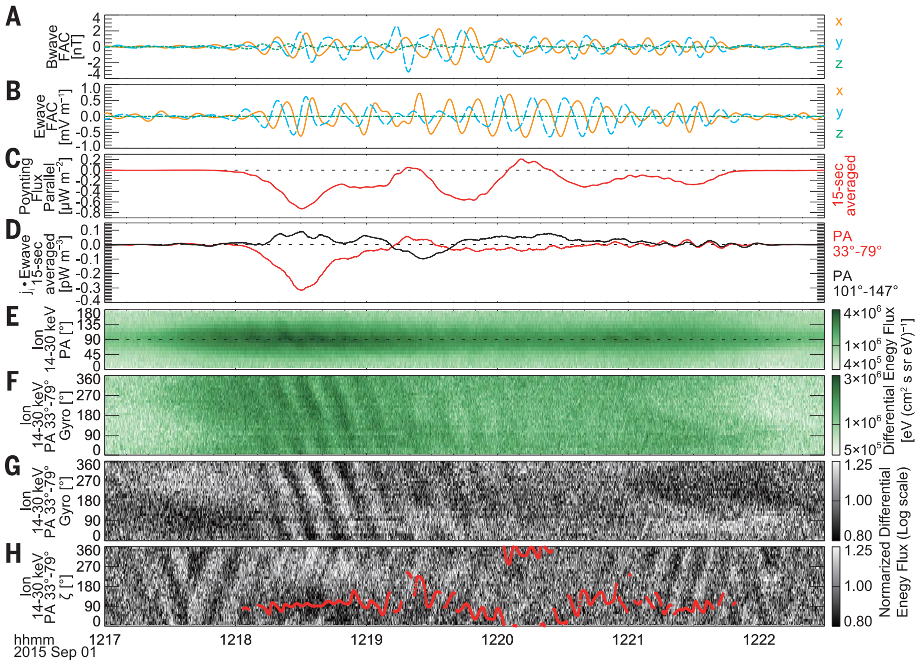

Fig. 2. Wave fields and hot ions (14 to 30 keV), averaged over all four spacecraft. (**A**) Wave magnetic field $\mathbf{B}_{wave}$. (**B**) Wave electric field $\mathbf{E}_{wave}$. (**C**) 15-s averaged Poynting flux **S** parallel to the background magnetic field. (**D**) 15-s averaged dot product of ion current $\mathbf{j}_i$ (14 to 30 keV) and $\mathbf{E}_{wave}$. (**E** and **F**) Pitch-angle (PA) and gyro phase spectrograms, respectively, of ion differential energy fluxes. (**G** and **H**) Gyro and relative phase (ζ) spectrograms, respectively, of normalized differential energy fluxes. Red dots mark the direction of $\mathbf{E}_{wave}$ when the amplitudes of $\mathbf{B}_{wave}$ and $\mathbf{E}_{wave}$ in the *x-y* plane of the field-aligned coordinate system were larger than 0.25 nT and 0.2 mV m^{-1}, respectively. The gyro and ζ spectrograms were constructed by using ions with pitch angles of 33.25° to 78.75°.

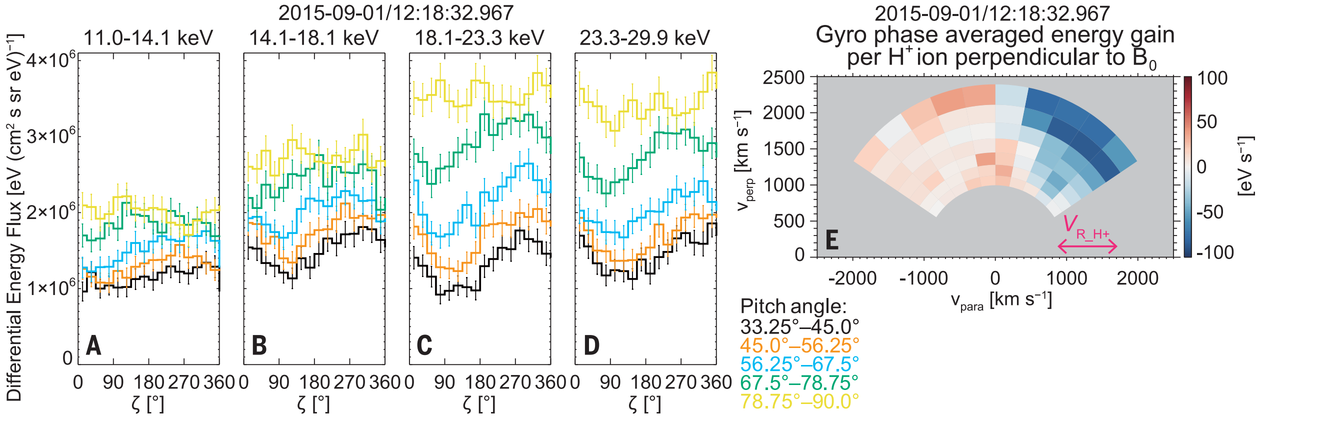

Fig. 3. Agyrotropy and energy gain of hot H$^+$. (**A** to **D**) Relative phase angle (ζ) distributions in 15-s averages of ion differential energy fluxes centered at 12:18:32.967 UT, split into pitch-angle bins from 33.25° to 90.0°. Distributions are separated by energy (A) 11.0 to 14.1 keV, (B) 14.1 to 18.1 keV, (C) 18.1 to 23.3 keV, and (D) 23.3 to 29.9 keV; error bars are 2σ. (**E**) Distribution for a 15-s gyro phase–averaged energy gain, perpendicular to the background magnetic field $\mathbf{B}_0$, per H$^+$ ion in the energy range of 5.1 to 29.9 keV in the velocity space: ion velocity parallel (v_{para}) and perpendicular (v_{perp}) to $\mathbf{B}_0$ plane.

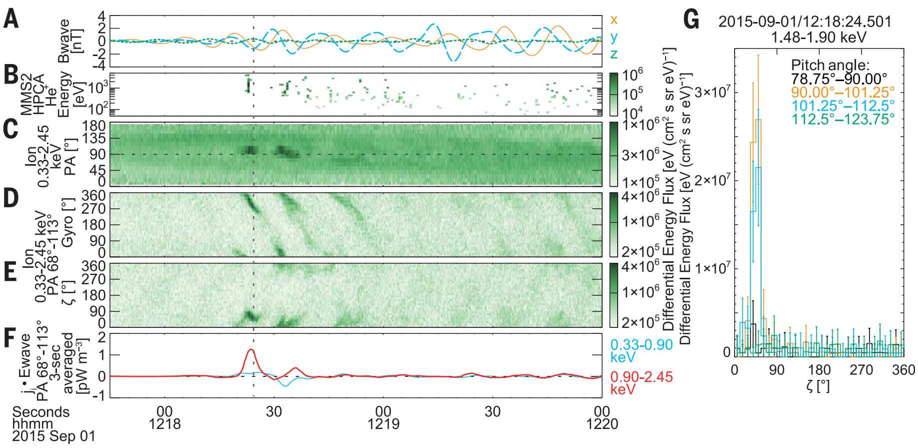

Fig. 4. Phase-bunched ions near the beginning of the wave event. (**A**) Wave magnetic field $\mathbf{B}_{wave}$. (**B**) Energy-time spectrogram of He$^+$. (**C** to **E**) Pitch-angle, gyro, and relative phase (ζ) spectrograms, respectively, of ion differential energy fluxes (0.33 to 2.45 keV). (**F**) $\mathbf{j}_i \cdot \mathbf{E}_{wave}$ averaged over 3 s. (**G**) ζ distributions of 1.05-s average of ion differential energy fluxes observed at 12:18:24.501 UT (vertical gray dashed line) by one spacecraft (MMS4) centered in pitch-angle bins from 78.75° to 123.75° and covering the energy bin 1.48 to 1.90 keV; error bars are 2σ. (C) and (D) were constructed by using ions with pitch angles of 67.5° to 112.5°.

higher than previous observation of bunched He$^+$ after a wave event (*20*). Positive $\mathbf{j}_i \cdot \mathbf{E}_{wave}$ around 12:18:24 UT (Fig. 4F) indicates that the He$^+$ ions with the highest flux in the event were being accelerated by $\mathbf{E}_{wave}$. In contrast to hot H$^+$ (Fig. 3, B to D), a sharp peak of ion fluxes appeared at ζ ~ 45°, which is ~45° from $\mathbf{E}_{wave}$ (ζ ~ 90°) (Figs. 1C and 4G and fig. S6). This provides evidence for an interaction in which almost all He$^+$ ions were accelerated by $\mathbf{E}_{wave}$, although energization of He$^+$ itself has been reported from the 1980s (*21*, *22*). The parallel motion of He$^+$ opposite to the direction of $V_{R_{He^+}}$ is inconsistent with the cyclotron resonant acceleration, which has been considered as the most plausible candidate for He$^+$ energization perpendicular to $\mathbf{B}_0$ (*19*, *23*, *24*). Thus, the interaction must be of nonresonant type (*25*), a phenomenon that has not been simulated self-consistently. In cases in which the wave amplitude is large and the wave frequency is slightly different from the cyclotron frequency of the ion species, ions can be substantially accelerated over a time scale of approximately $\pi/|\Omega_i - \omega|$ because of slow rotation of the wave electric field as felt by the ions. Phase bunching is also predicted, if the ions are initially sufficiently cold. Simple test particle tracing by using the measured parameters can explain the observed pitch angle, accumulation in gyro phase, and most of the energization (fig. S7) (*16*).

Using MMS's high time-resolution measurements of ions with a full-sky field of view, together with composition-resolved ion measurements, we have quantitatively demonstrated the simultaneous occurrence of two concurrent energy transfers: one from hot anisotropic H$^+$ (the free-energy source) to the ion cyclotron wave via cyclotron resonance and the other from the wave to He$^+$ via nonresonant interaction (Fig. 1). This provides direct quantitative evidence for collisionless energy transfer between distinct particle populations via wave-particle interactions. Such measurements, including information on the gyro phase of energetic charged particles relative to wave fields, provide the capability to unambiguously identify which types of wave-particle interaction are occurring.

REFERENCES AND NOTES

1. R. B. Horne *et al.*, *Nature* **437**, 227–230 (2005).
2. G. D. Reeves *et al.*, *Science* **341**, 991–994 (2013).
3. R. M. Thorne *et al.*, *Nature* **504**, 411–414 (2013).
4. T. Chang *et al.*, *Geophys. Res. Lett.* **13**, 636–639 (1986).
5. V. Jordanova *et al.*, *J. Geophys. Res.* **111** (A11), A11S10 (2006).
6. D. Mourenas, A. V. Artemyev, Q. Ma, O. V. Agapitov, W. Li, *Geophys. Res. Lett.* **43**, 4155–4163 (2016).
7. Y. Y. Shprits, A. Kellerman, N. Aseev, A. Y. Drozdov, I. Michaelis, *Geophys. Res. Lett.* **44**, 1204–1209 (2017).
8. N. P. Meredith, R. B. Horne, R. R. Anderson, *J. Geophys. Res.* **106** (A7), 13,165–13,178 (2001).
9. Y. Miyoshi *et al.*, *J. Geophys. Res.* **108** (A1), 1004 (2003).
10. R. C. Allen *et al.*, *J. Geophys. Res. Space Phys.* **121**, 6458–6479 (2016).
11. M. P. Gough, P. J. Christiansen, K. Wilhelm, *J. Geophys. Res.* **95**, 12,287–12,294 (1990).
12. H. Fukuhara *et al.*, *Earth Planets Space* **61**, 765–778 (2009).
13. Y. Katoh *et al.*, *Ann. Geophys.* **31**, 503–512 (2013).
14. M. Shoji *et al.*, *Geophys. Res. Lett.* **44**, 8730–8738 (2017).
15. J. L. Burch, T. E. Moore, R. B. Torbert, B. L. Giles, *Space Sci. Rev.* **199**, 5–21 (2016).
16. Materials and methods are available as supplementary materials.
17. Y. Omura *et al.*, *J. Geophys. Res.* **115** (A7), A07234 (2010).
18. C. Pollock *et al.*, *Space Sci. Rev.* **199**, 331–406 (2016).
19. C. G. Mouikis *et al.*, *Geophys. Res. Lett.* **29**, 74-1 (2002).
20. B. H. Mauk, C. E. McIlwain, R. L. McPherron, *Geophys. Res. Lett.* **8**, 103–106 (1981).

21. D. T. Young *et al*., *J. Geophys. Res.* **86** (A8), 6755–6772 (1981).
22. A. Roux *et al*., *J. Geophys. Res.* **87** (A10), 8174–8190 (1982).
23. J. C. Zhang *et al*., *J. Geophys. Res.* **115**, A06212 (2010).
24. J. C. Zhang *et al*., *J. Geophys. Res.* **116** (A11), A11201 (2011).
25. J. Berchem, R. Gendrin, *J. Geophys. Res.* **90** (A11), 10,945–10,960 (1985).

ACKNOWLEDGMENTS

We thank the entire MMS team and instrument leads for data access and support. We acknowledge J.-A. Sauvaud, V. N. Coffey, J. C. Dorelli, L. A. Avanov, B. Lavraud, M. O. Chandler, and C. Schiff for their valuable roles in providing instrumentation and data production/quality for the Fast Plasma Investigation. We also gratefully acknowledge E. Grimes and the development team of the Space Physics Environment Data Analysis System (SPEDAS) software for their fruitful efforts in providing this software for our use. **Funding:** This research was supported by the NASA MMS Mission in association with NASA contract NNG04EB99C, and by Grants-in-Aid for Scientific Research (17H06140 to N.K. and Y.S.; 15H05747 to M.K., Y.M., and Y.K.; 15H05815 to M.S., Y.M., and Y.K.; 17K14402 to M.S.; 16H06286 to Y.M.; and 15H03730 to Y.K.) of the Japan Society for the Promotion of Science (JSPS). D.J.G. is supported by the NASA MMS Mission Guest Investigators program. IRAP contributions to Fast Plasma Investigation on MMS were supported by CNES and CNRS. Support for R.J.S.'s effort was provided under subcontract with the University of New Hampshire, in turn under contract from SwRI and NASA. **Author contributions:** N.K. conceived and designed the study, found this event from the data, analyzed the data, and wrote the initial draft. M.K. and M.S. contributed to the design of the study and interpretation of the results. Y.M. oversaw the production of the dataset and discussed its interpretation. H.H. contributed to interpretation of the result and to writing. S.N. contributed to the design of the study and interpretation of the result and prepared Fig. 1. Y.K. contributed to interpretation of the results. Y.S. led Japanese contribution to the development of FPI-DIS on the MMS spacecraft used to make the plasma measurements. S.Y. contributed to the development of FPI. D.J.G. assisted with the interpretation and analysis of the high-resolution plasma data and with the preparation of the paper. A.F.V. contributed to the FPI analysis codes and to the interpretation of the results. B.L.G. led the calibration and operation of FPI and to the development of the scientific data products and is responsible for the data. T.E.M. led the design of FPI and its Instrument Data Processing Unit and consulted in their development, calibration, and operation and in the writing. W.R.P. contributed to the calibration and operation of FPI and to the development of the scientific data products. C.J.P. led the development of FPI. C.T.R. supervised the building of the magnetometer on MMS, its calibration and data processing, and assisted in the writing. R.J.S. was responsible for the in-flight calibration of the fluxgate magnetometers. S.A.F. led the development of the Hot Plasma Composition Analyzer on MMS and is responsible for the data. J.L.B. led the MMS mission and assisted in the writing. **Competing interests:** The authors declare no competing interests. **Data and materials availability:** The MMS data can be accessed from the MMS Science Data Center at https://lasp.colorado.edu/mms/sdc/public. We used the Level-2 data from the FGM survey (located in fgm/srvy/l2/scpot); FPI-DIS burst (fpi/brst/l2/dis-dist); EDP fast survey (edp/fast/l2/scpot); and HPCA burst (hpca/brst/l2/ion, hpca/brst/l2/moments), all from the period 12:15:28 to 12:24:00 UT on 1 September 2015. The Space Physics Environment Data Analysis System (SPEDAS) software used to download and analyze the data are available from http://themis.ssl.berkeley.edu/socware/bleeding_edge/spdsw_r24826_2018-03-02.zip. The Kyoto University Plasma Dispersion Analysis Package (KUPDAP) that was used to calculate the dispersion relation of the cyclotron wave is available from http://space.rish.kyoto-u.ac.jp/software.

SUPPLEMENTARY MATERIALS

www.sciencemag.org/content/361/6406/1000/suppl/DC1
Materials and Methods
Figs. S1 to S7
References (*26*–*35*)

5 September 2017; accepted 4 July 2018
10.1126/science.aap8730

Science

Direct measurements of two-way wave-particle energy transfer in a collisionless space plasma

N. Kitamura, M. Kitahara, M. Shoji, Y. Miyoshi, H. Hasegawa, S. Nakamura, Y. Katoh, Y. Saito, S. Yokota, D. J. Gershman, A. F. Vinas, B. L. Giles, T. E. Moore, W. R. Paterson, C. J. Pollock, C. T. Russell, R. J. Strangeway, S. A. Fuselier and J. L. Burch

Science **361** (6406), 1000-1003.
DOI: 10.1126/science.aap8730

Two-step energy transfer in space plasma

Plasmas are ionized gases that contain negative electrons, positive ions, and electromagnetic fields. These constituents can oscillate in position over time, carrying energy as plasma waves. In principle, such waves could transfer energy between two different ion populations. Kitamura *et al.* analyzed data from the Magnetospheric Multiscale mission, a group of four spacecraft that are flying in tight formation through Earth's magnetosphere. They discovered an event in which energy was transferred from hydrogen ions to plasma waves and then from the waves to helium ions. This energy transfer process is likely to occur in many other plasma environments.

Science, this issue p. 1000